Towards a Heuristic Path Loss Model for RIS Links

Lorenz H. W. Loeser[(1)] and Thomas Kürner*[(1)]
(1) Institute for Communications Technology, Technische Universität Braunschweig, Germany

Abstract

The continuously increasing demand for higher data rates drives the exploration of low terahertz (THz) frequency bands for mobile communications, leveraging their large available bandwidths. To reduce dependency on line-of-sight (LOS), the concept of reflective intelligent surfaces (RISs) has emerged as a promising technology. By reconfiguring the electromagnetic environment, RIS alters the channel, requiring novel approaches to model key parameters such as path gain. To address this, an approach based on the bistatic radar equation is proposed, which accounts for the altered path gain progression due to near field effects.

1 Introduction

The ever-growing demand for higher data transmission rates is driving the transition to elevated frequency bands, particularly the lower terahertz (THz) range, spanning from 0.1 THz to 1 THz. This spectrum offers vast bandwidth, making it feasible to achieve peak data rates in the terabit-per-second regime [1]. However, wireless communication at these frequencies encounters multiple challenges. One major issue is the pronounced attenuation of signals during propagation, which necessitates the use of highly directional antenna systems to compensate for these losses [1]. Furthermore, the absence of a line-of-sight (LOS) path between the transmitter (TX) and receiver (RX) can critically degrade the communication link's reliability within this frequency range due to the narrow beam widths [1].

A promising solution to mitigate LOS dependency while simultaneously enhancing network efficiency and overall performance is the deployment of reflective intelligent surface (RIS) technology [2]. A RIS is usually composed of numerous tunable sub-wavelength unit cells that enable dynamic phase control of impinging electromagnetic waves upon reflection. By leveraging this capability, RISs can alter the propagation environment, for instance, by introducing anomalous reflections to steer signals in desired directions [2]. To effectively integrate RIS into communication scenarios, accurate models for predicting key channel parameters, such as path gain, are essential. However, path gain estimation is challenging due to the unique characteristics of the TX-RIS-RX cascaded link, where participants may operate within the near field region of the RIS. This is due to large RIS dimensions D relative to small wavelengths λ at high frequencies, which results in high values of the Fraunhofer distance d_{FH} serving as the conventional border between near and far field.

$$d_{\mathrm{FH}} = \frac{2D^2}{\lambda} \tag{1}$$

Existing methods to model the path gain of a RIS link include analytical approaches. For example, in [3] every propagation path for every single unit cell is accounted for. This necessitates precise knowledge about the RIS such as the complex reflection coefficients and limits the model to reflectarray-type of RISs. In [4, 5] derivations of the electric fields in the presence of a RIS are provided, introducing high complexity when only the path gain is desired. Inspired by previous measurements, this paper presents a straightforward path gain model based upon the bistatic radar equation, adapted to account for near field effects. Additionally, models for the radar cross section (RCS) of a RIS and the influence of illumination are provided.

2 Path Gain Model

Throughout this paper, channel reciprocity is assumed, meaning that the path gains for the TX-RIS-RX link and for the RX-RIS-TX link are equal. This holds true if the RIS state remains unchanged when comparing the two links, provided that the RIS itself is composed of reciprocal materials - a condition that is met in the vast majority of cases [6].

In previous works [7, 8], results from a measurement campaign using a non-reconfigurable, passive RIS designed for far field beamforming with perpendicular incidence and anomalous reflection towards 30° at 304 GHz are presented. In that study, the conventional bistatic radar equation models the path gain of the RIS-assisted link, as shown in (2). The gain refers to the propagation channel, excluding antenna gains.

$$G_{\mathrm{Radar}} = \sigma_{\mathrm{RIS}} \cdot \frac{\lambda^2}{(4\pi)^3} \frac{1}{d_{\mathrm{TX,RIS}}^2 d_{\mathrm{RIS,RX}}^2} \tag{2}$$

σ_{RIS} is the RCS of the RIS, λ denotes the wavelength and $d_{\mathrm{TX,RIS}}$ and $d_{\mathrm{RIS,RX}}$ represent the distances between the TX and RIS, and between the RIS and RX, respectively. (2) is based on the radar equation which is derived for the far field [9]. However, it has been shown that it is a valid

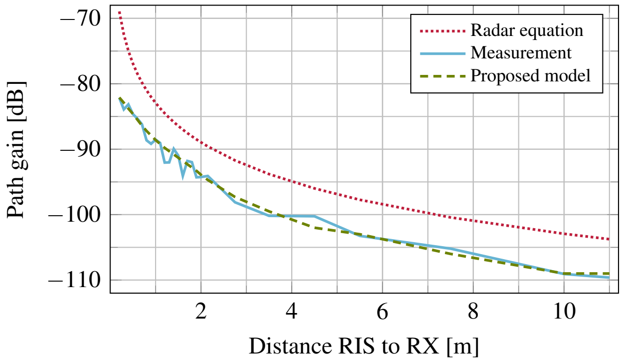

Figure 1. Measured path gain for TX-RIS-RX link over varying distance between RIS and RX for fixed distance between TX and RIS from [7]. Path gain as predicted by conventional bistatic radar equation (2) and proposed model (12).

tool for path gain prediction even at distances significantly shorter than the Fraunhofer distance [7, 10]. This can be observed in Fig. 1, which illustrates the measured path gain for the TX-RIS-RX link over a varying distance between RIS and RX as well as the path gain modeled by the conventional radar equation (2) and the adjusted radar equation (12), the latter of which is proposed in this paper. Disregarding the offset, stemming from alignment errors, beam squint, and measurement inaccuracies, a high degree of similarity in the curve progressions of radar equation and measurement for distances greater than 1 m is observable, thus confirming the fundamental suitability of the bistatic radar equation for path gain prediction. Nevertheless, below this distance the radar equation tends to overestimate the path gain. To address this, a distance-dependent adjustment of the power loss exponents—specifically, the exponents of $d_{\mathrm{TX,RIS}}$ and $d_{\mathrm{RIS,RX}}$, respectively—is proposed. In the conventional radar equation, these exponents have a fixed value of two.

2.1 Adjusted Radar Equation

The adjustment of the exponents p_{TX} and p_{RX} of $d_{\mathrm{TX,RIS}}$ and $d_{\mathrm{RIS,RX}}$ as a function of distance will result in an altered, distance-dependent progression of the path gain prediction. Therefore, the objective is to reduce the distance-dependency of the offset seen in Fig. 1, rather than eliminating the offset itself. A fixed adjustment of the power loss exponents, independent of the distance, similar to the floating intercept or α-β model, is not suitable, since the exponents must remain at two for sufficiently large distances. The adjustment of the power loss exponents is based on three distances: the Fraunhofer distances of TX and RX $d_{\mathrm{FH,X}}$ with $\mathrm{X} \in (\mathrm{TX};\mathrm{RX})$ and k times the Fraunhofer distance of the RIS $k \cdot d_{\mathrm{FH,RIS}}$. k is chosen according to measurement results to $k \in [0.1; 0.3]$ such that $k \cdot d_{\mathrm{FH,RIS}}$ represents the transition distance at which the traditional radar equation begins to overestimate the path gain. Here, $d_{\mathrm{FH,X}} < k \cdot d_{\mathrm{FH,RIS}}$ is assumed.

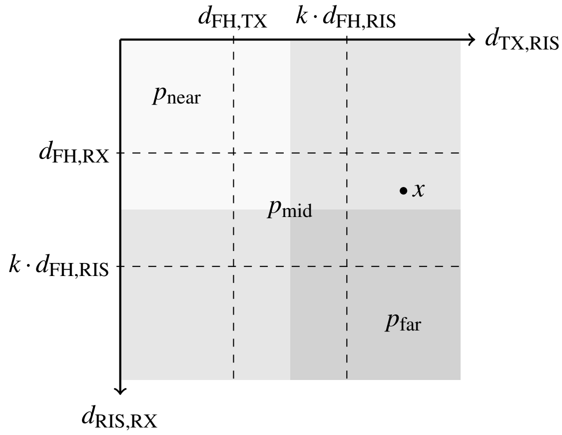

Figure 2. Visualization of the exponent adjustment approach.

Fig. 2 visualizes these distances as dashed lines along two axes: $d_{\mathrm{TX,RIS}}$ and $d_{\mathrm{RIS,RX}}$. The two-dimensional space represents all possible $(d_{\mathrm{TX,RIS}}; d_{\mathrm{RIS,RX}})$-tuples. For p_{TX}, i.e. $d_{\mathrm{TX,RIS}}$, the columns are of importance and for p_{RX}, i.e. $d_{\mathrm{RIS,RX}}$, the rows are of importance. The exponents p_{near}, p_{mid} and p_{far} correspond to the regimes, i.e. columns and rows, defined by the dashed lines. Given a certain distance between TX and RIS $d_{\mathrm{TX,RIS}}$, the corresponding gray shade illustrates the region in which specific exponents must be used to calculate the desired power loss exponent p_{TX}. The same applies to RX. This is done using

$$p_{\mathrm{X}} = w_{1,\mathrm{X}} \cdot p_{1,\mathrm{X}} + w_{2,\mathrm{X}} \cdot p_{2,\mathrm{X}}. \tag{3}$$

Here, $p_{1,\mathrm{X}}$ is the exponent of the dashed region within which $(d_{\mathrm{TX,RIS}}; d_{\mathrm{RIS,RX}})$ resides, for $\mathrm{X} \in (\mathrm{TX};\mathrm{RX})$ respectively. $p_{2,\mathrm{X}}$ is the exponent of the dashed tile which is nearest, as indicated by the gray-shaded regime, again for $\mathrm{X} \in (\mathrm{TX};\mathrm{RX})$ respectively. For example, for the $(d_{\mathrm{TX,RIS}}; d_{\mathrm{RIS,RS}})$-tuple x in Fig. 2, this results in $p_{1,\mathrm{TX}} = p_{\mathrm{far}}$, $p_{2,\mathrm{TX}} = p_{\mathrm{mid}}$, $p_{1,\mathrm{RX}} = p_{\mathrm{mid}}$ and $p_{2,\mathrm{RX}} = p_{\mathrm{near}}$. The weights $w_{1,\mathrm{X}}$ and $w_{2,\mathrm{X}}$ are determined by logistic functions which ensure a smooth transition of the power loss exponents:

$$\begin{aligned}
w_{1,\mathrm{TX}} &= \frac{1}{1+e^{-s\cdot(d_{\mathrm{TX,RIS}}-d_{\mathrm{dash,TX}})}},\\
w_{1,\mathrm{RX}} &= \frac{1}{1+e^{-s\cdot(d_{\mathrm{RIS,RX}}-d_{\mathrm{dash,RX}})}},\\
w_{2,\mathrm{X}} &= 1 - w_{1,\mathrm{X}}.
\end{aligned} \tag{4}$$

$d_{\mathrm{dash,TX}}$ and $d_{\mathrm{dash,RX}}$ correspond to the distances associated with the dashed lines within the shaded regimes. Depending on the position of $(d_{\mathrm{TX,RIS}}; d_{\mathrm{RIS,RX}})$ they are chosen to be either $d_{\mathrm{FH,X}}$ or $k \cdot d_{\mathrm{FH,RIS}}$. Exemplary for x, this results in $d_{\mathrm{dash,TX}} = k \cdot d_{\mathrm{FH,RIS}}$ and $d_{\mathrm{dash,RX}} = d_{\mathrm{FH,RX}}$. s is a parameter of the logistic function that allows for the adjustment of the steepness of the transition.

2.2 Bistatic RIS RCS

The bistatic RCS of the RIS is a key component of the radar eqation. Obtaining it is challenging since its value depends on the technology used for the RIS, its geometric dimensions, the states of the unit cells, the incidence, and scattering angles for which the bistatic RCS is to be obtained. The usual approach is to use full-wave electromagnetic simulations, as done in [8, 11]. However, this is a tedious process, especially as a new simulation is required every time the RIS state changes. The upper border of the achievable bistatic RCS of a RIS for a given set of angles is determined by the RCS of a perfect electric conductor (PEC) plate of equal size in the specular case. This is because a perfectly conducting surface reflects the entire wave without losses. The RCS of a PEC plate σ_{PEC} with length L and width W with perpendicular incidence and specular reflection is given by [9]

$$\sigma_{\mathrm{PEC}} = \frac{4\pi}{\lambda^2} \cdot (L \cdot W)^2. \tag{5}$$

The RCS of a RIS σ_{RIS} has to lie below this value. Additionally, it depends on the incidence and reflection angles $\psi_{\mathrm{RIS,TX}}$ and $\psi_{\mathrm{RIS,RX}}$ for which the RIS is designed. A simple approach to modeling the RCS of a RIS is to reduce σ_{PEC} by the cosine of the incidence and reflection angles, which may be explained by the projection of the area that contributes to scattering. Furthermore, the RIS efficiency, η_{RIS}, is introduced to account for additional losses that depend on the nature of the RIS, such as phase discretization or whether the RIS is reconfigurable or static. For example, a higher phase discretization and a passive, non-reconfigurable RIS lead to a higher RIS efficiency due to a more precise reflection and the absence of parasitic effects from active components. This results in [12]

$$\sigma_{\mathrm{RIS}} = \sigma_{\mathrm{PEC}} \cdot \cos(\psi_{\mathrm{RIS,TX}}) \cdot \cos(\psi_{\mathrm{RIS,RX}}) \cdot \eta_{\mathrm{RIS}}. \tag{6}$$

This approach enables rapid modeling of the RCS without making assumptions about the specific RIS technology used. Furthermore, it aligns well with full-wave simulations presented in [8]. For the passive RIS designed for 304 GHz, with perpendicular incidence and 30° anomalous reflection, as studied in [7, 8], the values of η_{RIS} are 0.73, 0.58, and 0.26 for 3-bit, 2-bit, and 1-bit phase discretization, respectively. Similarly, for the reconfigurable 2-bit RIS at 24.5 GHz in [13], η_{RIS} is approximately 0.4. Naturally, more data for different RIS designs has to be acquired, but (7) serves as a reasonable first approximation.

$$\eta_{\mathrm{RIS,dB}} \approx -\left\{ \begin{array}{ll} 1.5\,\mathrm{dB}, & \text{3-bit} \\ 3\,\mathrm{dB}, & \text{2-bit} \\ 6\,\mathrm{dB}, & \text{1-bit} \end{array} \right\} - \left\{ \begin{array}{ll} 1\,\mathrm{dB}, & \text{reconf.} \\ 0\,\mathrm{dB}, & \text{static} \end{array} \right\} \tag{7}$$

2.3 Illumination Loss

Especially for narrow beam widths of the TX and RX, large RIS dimensions, and small distances $d_{\mathrm{TX,RIS}}$ and $d_{\mathrm{RIS,RX}}$, the illumination of the RIS impacts the path gain. To account for this effect, the approach taken here is similar to that in [3]. However, this approach eliminates the need for assumptions and considerations for every unit cell, as the behavior of the entire RIS is modeled by its RCS. First, the normalized main lobes of the TX and RX are modeled as [3]

$$G_{\mathrm{X,norm}}(\psi) = \cos^{q_{\mathrm{X}}}(\psi) \tag{8}$$

where ψ is the angle from the center of the main lobe and $\mathrm{X} \in (\mathrm{TX};\mathrm{RX})$. If the half power beam widths (HPBWs) $\psi_{\mathrm{HPBW,X}}$ of the main lobes are known, the exponents q_{X} can be calculated by

$$q_{\mathrm{X}} = \frac{\log(0.5)}{\log\left(\cos(\frac{\psi_{\mathrm{HPBW,X}}}{2})\right)}. \tag{9}$$

(9) is derived from $G_{\mathrm{X,norm}}(\frac{\psi_{\mathrm{HPBW,X}}}{2}) = 0.5$. Otherwise, if the HPBWs are not known, the exponents q_{X} can be determined using [3]

$$q = \frac{G_{\max}}{2} - 1 \tag{10}$$

where $G_{\mathrm{max,X}}$ are the maximum gains of the main lobes. (9) was found to represent the form of the main lobe of an antenna more accurately than (10), which can be attributed to the additional information used by the former. To incorporate the effect of illumination, the RIS surface is arbitrarily discretized into I discretization points. Assuming perfect alignment of the TX and RX towards the center of the RIS, the angle $\psi_{\mathrm{TX,RIS},i}$ between perfect alignment and the vector connecting the TX to a discretization point is determined for each discretization point i. $\psi_{\mathrm{RX,RIS,i}}$ is determined analogously. Using (8), the corresponding antenna gain values are calculated. The overall illumination efficiency η_{illu} is then obtained by averaging all gains over the discretization points:

$$\eta_{\mathrm{illu}} = \frac{\sum_i G_{\mathrm{TX,norm}}(\psi_{\mathrm{TX,RIS},i}) + G_{\mathrm{RX,norm}}(\psi_{\mathrm{RX,RIS},i})}{I}. \tag{11}$$

In summary, using (3) for the power loss exponents, (6) to model the bistatic RCS of the RIS, and (11) to account for the impact of illumination, the path gain G of a TX-RIS-RX link in both directions may be modeled by

$$G = \sigma_{\mathrm{RIS}} \cdot \frac{\lambda^2}{(4\pi)^3} \cdot \frac{1}{d_{\mathrm{TX,RIS}}^{p_{\mathrm{TX}}} d_{\mathrm{RIS,RX}}^{p_{\mathrm{RX}}}} \cdot \eta_{\mathrm{illu}}. \tag{12}$$

This assumes known positions, a narrowband signal, and perfect alignment. Additionally, the RIS must be designed for the angles corresponding to the TX and RX positions.

2.4 Derived Parameters

The determination of the most suitable channel model parameters for the measurement corresponding to Fig. 1 is done by a parameter sweep. The mean difference between measured and modeled path gain serves as the objective function. Since the constant offset is attributed to effects not yet respected in the model, this shift is part of the sweep as well. This yields $k = 0.2$, $p_{\text{near}} = 1$, $p_{\text{mid}} = 1.5$, $s = 4$ and a shift of 5.2 dB. The resulting path gain curve is shown in Fig. 1, displaying substantial agreement. Naturally, further measurements with other RISs should be conducted to corroborate this approach and mitigate overfitting.

3 Conclusion

In this paper a measurement-based, straightforward path gain model for a TX-RIS-RX link is proposed. This model is based on the bistatic radar equation, which has been shown to be a suitable prediction tool in principle in the context of previous measurement campaigns. To account for different power scaling due to near field effects, a distance-dependent adjustment of the power loss exponents is introduced, yielding significantly better agreement for locations close to the RIS. Additionally, the illumination loss is accounted for. To increase the generality of channel parameters, further measurements must be conducted with other RISs. To develop a complete channel model, future work aims to expand this model to include the beam squint effect and the impact of misalignments, both by means of measurements. Furthermore, statistical channel parameters have to be added by means of calibrated simulations.

4 Acknowledgements

This work has been performed within the TERRAMETA project. The TERRAMETA project has received funding from the Smart Networks and Services Joint Undertaking (SNS JU) under the European Union's Horizon Europe research and innovation programme under Grant Agreement No 101097101, including top-up funding by UK Research and Innovation (UKRI) under the UK government's Horizon Europe funding guarantee.

References

[1] C. Han, Y. Wang, Y. Li, Y. Chen, N. A. Abbasi, T. Kürner, and A. F. Molisch, "Terahertz Wireless Channels: A Holistic Survey on Measurement, Modeling, and Analysis," *IEEE Communications Surveys & Tutorials*, vol. 24, no. 3, pp. 1670–1707, 2022.

[2] S. Gong, X. Lu, D. T. Hoang, D. Niyato, L. Shu, D. I. Kim, and Y.-C. Liang, "Toward Smart Wireless Communications via Intelligent Reflecting Surfaces: A Contemporary Survey," *IEEE Communications Surveys & Tutorials*, vol. 22, no. 4, pp. 2283–2314, 2020.

[3] W. Tang, X. Chen, M. Chen, J. Dai, Y. Han, M. Di Renzo, S. Jin, Q. Cheng, and T. J. Cui, "Path Loss Modeling and Measurements for Reconfigurable Intelligent Surfaces in the Millimeter-Wave Frequency Band," *IEEE Transactions on Communications*, vol. 70, no. 9, pp. 6259–6276, 2022.

[4] V. Degli-Esposti, E. M. Vitucci, M. D. Renzo, and S. A. Tretyakov, "Reradiation and scattering from a reconfigurable intelligent surface: A general macroscopic model," *IEEE Transactions on Antennas and Propagation*, vol. 70, no. 10, pp. 8691–8706, 2022.

[5] F. H. Danufane, M. Di Renzo, J. de Rosny, and S. Tretyakov, "On the Path-Loss of Reconfigurable Intelligent Surfaces: An Approach Based on Green's Theorem Applied to Vector Fields," *IEEE Transactions on Communications*, vol. 69, no. 8, pp. 5573–5592, 2021.

[6] W. Tang, X. Chen, M. Z. Chen, J. Y. Dai, Y. Han, S. Jin, Q. Cheng, G. Y. Li, and T. J. Cui, "On channel reciprocity in reconfigurable intelligent surface assisted wireless networks," *IEEE Wireless Communications*, vol. 28, no. 6, pp. 94–101, 2021.

[7] L. H. W. Loeser, S. Matos, and T. Kürner, "Channel measurements involving passive RIS at 300 GHz," in *IEEE Eur. Conf. Antennas Propag.*, (Stockholm, Sweden), 2025. accepted.

[8] G. C. Alexandropoulos, B. K. Jung, P. Gavriilidis, S. Matos, L. H. W. Loeser, V. Elesina, A. Clemente, R. D'Errico, L. M. Pessoa, and T. Kürner, "Characterization of indoor ris-assisted channels at 304 ghz: Experimental measurements, challenges, and future directions," 2024. Submitted to IEEE Vehicular Technology Magazine.

[9] C. A. Balanis, *Antenna Theory - Analysis and Design*. New Jersey: John Wiley & Sons, 3rd ed., 2005.

[10] E. Björnson, O. T. Demir, and L. Sanguinetti, "A Primer on Near-Field Beamforming for Arrays and Reconfigurable Intelligent Surfaces," in *Proc. 2021 55th Asilomar Conference on Signals, Systems, and Computers*, pp. 105–112, 2021.

[11] Y. Liu and C. D. Sarris, "Efficient propagation modeling for communication channels with reconfigurable intelligent surfaces," *IEEE Antennas and Wireless Propagation Letters*, vol. 21, no. 10, pp. 2120–2124, 2022.

[12] G. C. Alexandropoulos, A. Clemente, S. Matos, R. Husbands, S. Ahearne, Q. Luo, V. Lain-Rubio, T. Kürner, and L. M. Pessoa, "Reconfigurable intelligent surfaces for thz: Hardware design and signal processing challenges," in *2024 18th European Conference on Antennas and Propagation (EuCAP)*, pp. 1–5, 2024.

[13] L. G. da Silva, Z. Chu, P. Xiao, and A. Cerqueira S, "A varactor-based 1024-element ris design for mmwaves," *Frontiers in Communications and Networks*, vol. 4, 2023.